International Journal of
INTELLIGENT SYSTEMS AND APPLICATIONS IN ENGINEERING
ISSN:2147-6799 www.ijisae.org Original Research Paper

Identification of Pneumonia in Chest X-Ray Images using Bio-Inspired Optimization Based LSTM

Gaurav Kumar Rajput[1], **Alka Singh**[2], **Saravana Kumar**[3], **Devendra Kumar Doda**[4]

Submitted: 17/04/2023 **Revised**: 14/06/2023 **Accepted**: 27/06/2023

Abstract: Pneumonia, a potentially dangerous respiratory condition, affects millions of people worldwide. Pneumonia has to be identified as early and precisely as possible in order to successfully treat and care for patients. Although the diagnosis of pneumonia is often made via chest X-ray (CXR) imaging, doing so may be time-consuming and complicated for medical professionals. This article proposes a novel strategy for the identification of pneumococcal infection in CXR images using bio-inspired optimization based Long Short-Term Memory (BIO-LSTM) methodologies. Bio-inspired optimization techniques are used, such as Stud Genetic Algorithm (SGA) to enhance the performance of the LSTM model. CXR images were compiled into a comprehensive Kaggle dataset from some sources. To provide an accurate portrayal of the target pathophysiology, the dataset included a wide variety of pneumonia and non-pneumonia patients. The dataset received a preprocessing phase utilizing Sparse Auto-Encoder (SAE) methods to enhance its quality and utility. A popular feature extraction method is the Gabor filter, which takes inspiration from the human visual system. These algorithms optimize the LSTM design and its parameters by simulating the behavior of natural systems, such as the development of genetic populations. A dataset of CXR including both normal and pneumonia patients is utilized to assess the suggested approach. Results from experiments show that the BIO-LSTM strategy for identifying pneumonia performs better than conventional approaches. According to this study's results, pneumonia may be identified more precisely and reliably by combining BIO-LSTM algorithms with the temporal information included in CXR images.

Keywords: *Pneumonia, Chest X-Ray (CXR), BIO-LSTM, Image, Patients*

1. Introduction

Inflammation of the lungs' air sacs is a typical feature of pneumonia, a respiratory illness. A chest X-ray of the patient may be examined, and particular anomalies can be identified to identify the presence and severity of the sickness [1]. One of the most common signs of pneumonia is consolidation on an X-ray of the chest. Consolidation happens when fluid or pus becomes trapped in the air-filled chambers of the lungs. It appears as dense or irregular opacities on the X-ray, which signify areas that are infected [2]. Infiltrates are regions of the lungs where the infection has become more prevalent. They may appear as hazy or fuzzy opacities on the X-ray, often in a lobar or segmental distribution [3]. Air bronchograms are a useful indicator of pneumonia on a CXR. These are bronchial tubes that are lined with hardened lung tissue and filled with air. The infection is seen on the X-ray as a branching pattern of black bronchi among the white opacities [4]. The location of the opacities that are shown on a CXR may also give information regarding the kind and severity of pneumonia that is present. In contrast to lobar pneumonia, which affects an entire lobe of the lung, bronchopneumonia often presents as diffuse opacities that are patchy and distributed across the lungs [5]. A condition known as pleural effusion is when there is an accumulation of fluid in the pleural space as a consequence of pneumonia. On a chest X-ray, the sharp angle that normally exists between the lung and the chest wall becomes softened or concealed due to pleural effusion. In addition to pneumonia, this is another observation that could be made about the patient [6]. The amount and location of the opacities shown on the X-ray may vary depending on the causative agent and stage of pneumonia. For instance, larger, more pronounced opacities may be seen in bacterial pneumonia whereas smaller, more widespread opacities may be present in viral pneumonia [7]. The initial stage in the diagnosis of pneumonia often involves a chest X-ray, but it's important to keep in mind that the findings are not always definitive. Occasionally, further imaging tests, such as a CT scan or clinical examination, may be necessary to determine the presence of pneumonia and determine its severity [8]. To analyze the pictures and provide a precise diagnosis, radiologists and other medical personnel skilled in reading chest X-rays

[1]*Assistant Professor, College of Computing Science and Information Technology, Teerthanker Mahaveer University, Moradabad, Uttar Pradesh, India, Email id: gauravrajput31@gmail.com*

[2]*Assistant Professor, Department of Master of Computer Application, Noida Institute of Engineering and Technology, Greater Noida, Uttar Pradesh, India, Email id: alkasingh.it@niet.co.in*

[3]*Assistant Professor, Department of Computer Science and Engineering, Presidency University, Bangalore, India, Email Id: saravanakumar.s@presidencyuniversity.in*

[4]*Associate Professor, Department of Electrical Engineeing, Vivekananda Global University, Jaipur, India, Email Id: devendra.doda@vgu.ac.in*

are essential. They can recognize the distinctive pneumonia-related symptoms and tell them apart from other lung anomalies thanks to their expertise [9]. It is important to remember that a CXR cannot identify the pneumonia-causing agent by itself. It may be necessary to do further diagnostic procedures, such as sputum cultures, blood tests, or molecular testing, to pinpoint the precise bacteria causing the illness [10]. This article proposes a novel strategy for the identification of pneumococcal infection in CXR images using bio-inspired optimization based Long Short-Term Memory (BIO-LSTM) methodologies.

2. Related Works

In the study [11], they identify the occurrence of COVID-19 in CXR images; a new BMO-CRNN model is developed. Several performance measures are analyzed to probe the experiment's results. The model's optimum performance was shown in simulations using BMO-CRNN. In research [12], they want to create a reliable model for extracting high-level characteristics of COVID-19 from CXR pictures, which would aid in timely diagnosis. Performance has been verified and compared to that of other methods, including more traditional machine learning and deep learning methods, meta-heuristics approaches, and chaotic maps. According to the available data, people infected with COVID-19 often have symptoms after a lung infection. Therefore, in certain areas where PCR is not easily accessible, CXR and chest CT may serve as a proxy. To exhibit that the suggested method yields state-of-the-art outcomes, we performed tests on three open-source datasets [13]. Research [14] provided a deep learning technology that, by combining the Xception neural network with LSTM, can automatically diagnose patients with pneumonia in X-ray pictures. The model starts by using the Xception network to extract deep features from the data, then it sends those features to the LSTM, where it is detected, and lastly, the most important characteristics are chosen. Second, the conventional cross-entropy loss is inadequate to rectify the imbalance of categories present in the samples used for the training set. On the already available datasets, the study has produced the desired outcomes when compared to the current technological approaches. And help clinicians improve their categorization accuracy for pediatric pneumonia. In research [15], they provide a novel metaheuristic-based fusion model for detecting COVID-19 from CXR. Some preprocessing, feature extraction, and classification procedures are included in the proposed model. We evaluate the suggested model's performance on the CXR image dataset from some angles. The results collected verified the provided model's higher presentation compared to state-of-the-art techniques. In research [16], they present a new methodology for predicting pneumonia and Covid-19 in the lungs based on chest X-rays. The components of the system include data set collection, picture enhancement, region of interest estimate that is both adaptive and precise, feature extraction, and illness prognosis. We have utilized two publicly accessible sets of CXR images to compile our data. The suggested approach is shown to be both resilient and efficient in experiments, outperforming previous best practices. Automatic diagnosis of COVID-19 is performed by thorough medication reports from medical pictures, to highlight coronavirus testing procedures and control community spread. Analysis of the suggested algorithm's performance in comparison to the state-of-the-art model demonstrates its superiority for COVID-19 detection segmentation and classification [17]. To correctly diagnose pneumonia from chest X-rays, a novel hybrid explainable deep learning system is suggested. The suggested hybrid process combines the strengths of ensemble convolutional networks with those of the Transformer Encoder algorithm [18]. The Hill-Climbing Algorithm-based CNN (CNN-HCA) model is a suggested optimization strategy for improving the CNN model's parameters to improve the CNN classifier's performance. Using a simulation analysis, we compare the proposed CNN-HCA model's performance to that of other hybridized classifiers, such as Particle Swarm Optimization [19]. Research [20] presented an Optimized Transfer Learning-based Approach for the Automatic Detection of COVID-19, which utilizes CXR images to provide a diagnosis based on an optimization technique applied to a total of twelve different CNN architectures. As shown by the experiments, the highest performance is attained by the DenseNet121 optimized design.

3. Methodology

The SAE was utilized to reduce noise, enhance image clarity, and extract relevant features. By training the SAE on a large set of unlabeled CXR images, the model learned to reconstruct the input data while capturing the salient features of the images. The encoded representations obtained from the SAE were then used as the input for subsequent feature extraction.

It is particularly effective in capturing texture information, which is crucial for identifying subtle patterns in CXR images. The Gabor filter bank was applied to the preprocessed images to extract discriminative features that represent the texture and structural characteristics associated with pneumonia. Multiple scales and orientations of the Gabor filters were used to ensure the extraction of relevant information across different spatial frequencies.

3.1. Dataset Descriptions

This study uses a Kaggle-obtained pneumonia dataset based on latter and frontal CXR imaging of chosen pediatric patients from the Women and Children's Medical Centre in Guangzhou. Patients in the dataset range in age from infants to young children. CXRs were taken as part of the regular medical treatment for the patients. 1341 normal CXR pictures and 3875 images with pneumonia serve as the training data. However, the test data includes 390 photos of pneumonia-infected CXR and 234 images of healthy CXR. Fig. 1 depicts an example of normal CXR, while CXR taken from a patient with pneumonia [21].

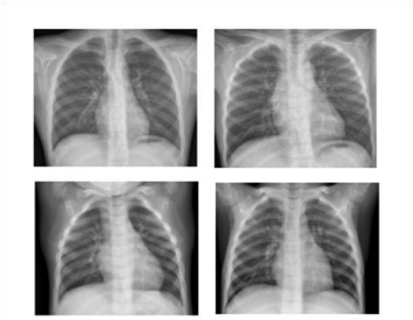

Fig. 1. Illustrations of CXR images [21]

3.2. Sparse Auto-Encoder

During network training, a sparse penalty *(g(x))* might be included in the role *Z* in place of solely minimizing the cost function *Z(x, f (g(x)))*, which calculates the disparity among *x* and *y=f (g(x))*. The AE's ability to express x with a limited number of *h* apparatus is improved by selecting the function g(x). The AE is referred to be an SAE when this occurs.

Fig. 2 depicts a sample SAE network to exhibit the aforementioned concepts. It consists of a core layer, which is the source of the h internal codes, and an equivalent numeral of encoding and decoding layers, which are both 2 in this particular figure. For SAE networks, a symmetric layout is required. There are M neurons in the encoder and M neurons in the decoder, where M is the length of the sampled signals. Each structural signal x, which is collected of M data points, is mapped onto K neurons in the middle layer. These K neurons correspond to the K interior apparatus h that are utilized to differentiate the signal. Note that $K \ll M$, indicating that the input variables have been transformed into new ones with lesser dimensions. To do this, two distinct structures are investigated concerning the primary SAE factors (explained in more detail in the article), namely the numeral of encoding/decoding layers & the size of the vector h. It should be noted that significant data regarding the structure's behavior is evaluated using the feature vector *h*.

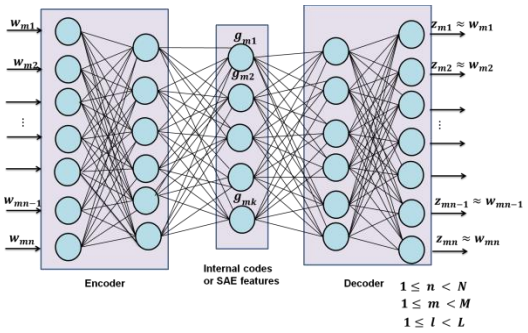

Fig. 2. SAE network.

3.3. Feature Extraction Using the Gabor Filter

An excellent tool for image processing, particularly in FR, is the Gabor filter. In the spatial domain, a composite sinusoidal hydroplane signal with a center frequency of f and an orientation θ of modulates a Gaussian kernel function, and this process is known as a Gabor filter.

$$H(w,z) = \frac{e^2}{\pi\gamma\eta} f\left(-\frac{w'^2+\gamma^2 z'^2}{2\sigma^2}\right) f^{(i2\pi ex'+\phi)}{}_{w'=w\cos+z\sin\theta z'=-w\sin\theta+z\cos\theta} \quad (1)$$

Where γ and η stand for the ratio between the center frequency and the Gaussian function's standard deviation σ, and ϕ denotes phase counteract.

The stripes in the function are controlled by the wavelength, with a higher frequency resulting in narrower stripes. The Gabor envelope's rotation is determined by the orientation, while the function's height is determined by its aspect ratio. When the aspect ratio is extremely high, the envelope's height is close to one pixel, and when the aspect ratio is very narrow, the height spreads over the whole picture. The size of the Gabor envelope is determined by the bandwidth, with a larger bandwidth resulting in a larger envelope and hence more possible stripes.

One of the numerous benefits of using a Gabor filter is that it is scale-, rotation-, and translation-invariant. The ability to use Gabor filters with varying frequencies and orientations makes them well-suited for extracting a wide variety of characteristics from an image, and they are also resilient against picture disruptions like changes in light.

Feature extraction for texture analysis and segmentation is aided by them greatly. While the orientation shifts to monitor texture in a certain direction, the Gaussian envelope standard deviation changes to regulate the size of the studied area in the image.

3.4. Bio-inspired optimization LSTM

Bio-inspired optimization LSTM (BIO-LSTM), is a cutting-edge method that combines the strength of optimization methods inspired by biological systems with the capabilities of LSTM networks. In a variety of applications, including time series prediction, natural

language processing, and sequential data analysis, this fusion of approaches attempts to increase the effectiveness and performance of LSTM models.

The incorporation of an optimization algorithm into the training process is a crucial component of BIO-LSTM. This approach uses iterative evaluation to direct the search for the best weights and biases for the LSTM network. This process is comparable to the biological systems' natural selection mechanism, where the more fit individuals have a higher chance of surviving and procreating.

Stud Genetic Algorithm (SGA):

- Development: The use of evolutionary computing approaches is widely supported. Fogel clarified the many benefits and drawbacks of each algorithm and its variations in 1995. An efficient solution to address the multidisciplinary optimization (MDO) issue was required as a result of the development of the multidisciplinary optimization discipline. SGA was thus established.
- Intent: The major goal of this was to create new children by mating the best member of the population with every other member. This does not use stochastic selection. The core of this method is the crossover operation. The common bit mutation with a low frequency is the mutation employed in this instance. Standard 2-point crossover and a decreased substitute consistent intersect were both explored.
- Performance: Several test functions were utilized to evaluate the SGA's functionality. Different difficulties arise from each collection of functions. The SGA does not use stochastic selection and keeps the conventional discrete bit format. The strategy is simple, yet it seems to be a potent tool for navigating challenging multimodal situations.
- Application: Power system optimization, data mining rule extraction optimization, computer-aided design (CAD) mobile robot path planning, flight control system design, pattern recognition, various scheduling problems, portfolio optimization, and multi-objective vehicle routing are just some of the many possible applications.

LTSM) network is a subset of artificial neural networks. It's a kind of recurrent neural network, a potent deep learning technology. Each LTSM stores the results of processing a sequence of any length (w_1, $w_{2,\ldots}$ w_s,...) in a single memory slot, much like a chain of repeating modules in a neural network. An example LTSM module's construction and operating principle are shown in Fig. 3.

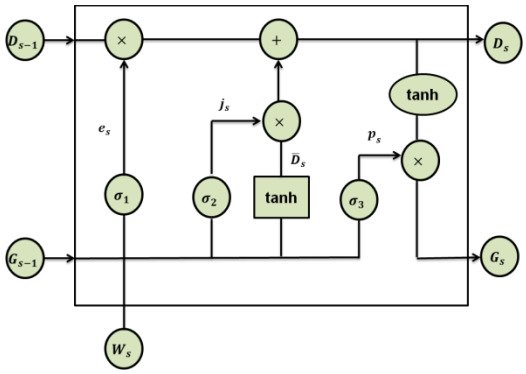

Fig. 3. An LSTM network module

The term "cell state" is used to describe the horizontal axis at the module's top. It travels in a straight line down the length of the chain, storing sequential data in an internal state and enabling the LSTM to retain information learned at later times. The gates stand for how data is filtered; they regulate the state of the cell by determining how much data is forgotten (the "forget gate"), how much is remembered (the "input gate"), and how much is revealed (the "output gate"). A sigmoid neural network layer and a point-wise multiplication operation make up each gate. The sigmoid layers generate integers in the range [0, 1] that indicate what fraction of the input data should be sent through. Getting a "zero" as a result implies rejecting everything, whereas getting a "one" means allowing everything. The LSTM component operates as follows. The initial phase of LSTM is to determine which previous states' information should be forgotten after getting the new information e_s in state s, using equation (2) to output a number inside [0, 1] from the forget gate.

$$e_s = \sigma_1(X_e.[g_{s-1}, w_s] + a_e), \quad (2)$$

When stored in cell state, $s-1$ is the output in states X_e and a_e. In this stage, the values updated in the cell state, such as j_s, are decided in the sigmoid layer σ_2 using a vector of potential values, such as $\widetilde{D}_s$, that is simultaneously produced by the tanh layer. Equation (3) then updates the new cell state D_s with the updated information from the old cell state.

$$D_s = e_s * D_{s-1} + j_s * \widetilde{D}_s \quad (3)$$

Which e_s and $\widetilde{D}_s$ are defined in equations (4 & 5)

$$e_s = \sigma_2\big(X_{j.}[g_{s-1}, w_s] + a_j\big), \quad (4)$$

$$.\widetilde{D}_s = \tanh(X_{d.}[g_{s-1}, w_s] + a_d), \quad (5)$$

Where $(X_{j,}a_j)$ and $(X_{d,}a_d)$ are the weight matrices for the input gate and memory cell state biases, respectively. The last step is to generate LSTM cell output values from the current state. The output gate P_s computes a fraction of the cell state to be outputted as a number between 0 and 1 using the sigmoid layer σ_3 layer's scaling of the vector state to the range [1, 1].

Multiplying these two integers in equations (6 & 7) serves as a variety of regulation and filtering before the result g_s is produced.

$$g_s = p_s * \tanh(D_s), \quad (6)$$

$$P_s = \sigma_3\left(X_{p.}[g_{s-1}, w_s] + a_p\right) \quad (7)$$

Where $X_{p.}$and a_p represent the weight matrix and output gate bias, respectively. Different writers have also proposed several LSTM variations. Different writers have also proposed several LSTM variations.

4. Results

Based on the True Positive (TP), True Negative (TN), False Positive (FP), and False Negative (FN) findings from the confusion matrix, the performance of the classifier is determined. The classifier has correctly predicted the real scenario if it returned TN or TP. In contrast, the classifier predicted incorrectly in the situations FP and FN.

The percentage of samples for which the suggested approach accurately predicted results is used to assess how accurate the system. The accuracy is calculated using the equation (8).

$$\text{Accuracy} = \frac{\text{TP+TN}}{\text{TP+TN+FP+FN}} \quad (8)$$

Fig. 4 displays comparable values for the accuracy metrics and makes it evident that the suggested technique can generate performance results that are better than those generated by the current research approaches. The suggested method's accuracy of 96% outperforms the results of the current ones, which include BIO-LSTM having a 65% accuracy rate, NN at 75.48%, KNN at 86.64%, and SVM at 98.27%. When classifying the data, the suggested technique outperformed existing techniques.

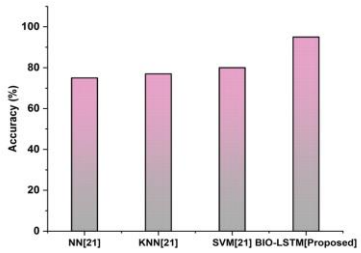

Fig. 4. Results of accuracy

Table 1. Numerical outcome of accuracy

	Accuracy (%)
NN[21]	75
KNN[21]	77
SVM[21]	80
BIO-LSTM[Proposed]	95

One of the most crucial standards for accuracy is precision, which is well-defined as the ratio of correctly classified cases to all instances of predictively positive data. The precision is calculated using equation (9).

$$\text{precision} = \frac{\text{TP}}{\text{TP+FP}} \quad (9)$$

Fig. 5 displays comparable values for the precision measures. With a 90% precision, the suggested method outperforms the currently used ones, which include BIO-LSTM (in precision (61%), KNN (82.48%), SVM (71.64%), and NN 88.27%). The proposed method achieved more data categorization precision than other methods currently in use.

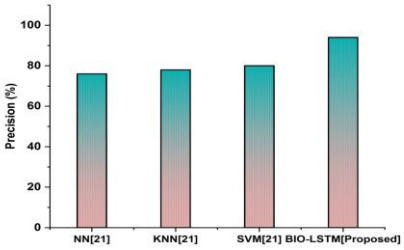

Fig.5. Results of precision

Table 2. Numerical outcome of precision

	Precision (%)
NN[21]	76
KNN[21]	78
SVM[21]	80
BIO-LSTM[Proposed]	94

The suggested model's sensitivity is its ability to recognize each important sample in a data collection. It is derived statistically by dividing the percentage of TPs by the total of TPs and FNs. The sensitivity is assessed using the equation (10).

$$\text{sensitivity} = \frac{\text{TP}}{\text{TP+FN}} \quad (10)$$

In Fig. 6 Sensitivity-wise, NN scores 64.35%, KNN.86%, SVM85.63%, and BIO-LSTM 90.08%.

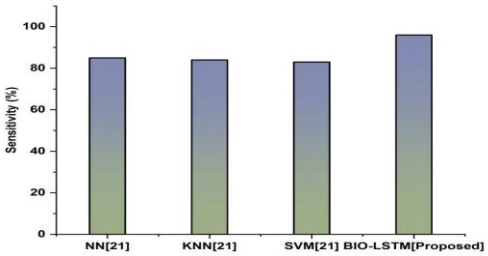

Fig. 6. Results of sensitivity

Table 3. Numerical outcome of sensitivity

	Sensitivity (%)
NN[21]	85
KNN[21]	84
SVM[21]	83
BIO-LSTM[Proposed]	96

The potential of a model to identify each important sample within a data collection is known as recall. The percentage of TPs divided by the sum of TPs and FNs is how it is statistically defined. The recall is calculated using equation (11).

$$\text{Recall} = \frac{\text{FN}}{\text{FN+TP}} \quad (11)$$

Comparative data for the recall metrics are shown in Fig. 7. Recall rates for BIO-LSTM (are 80.31%, KNN 70.14%, SVM 66.82%, and NN 87%.

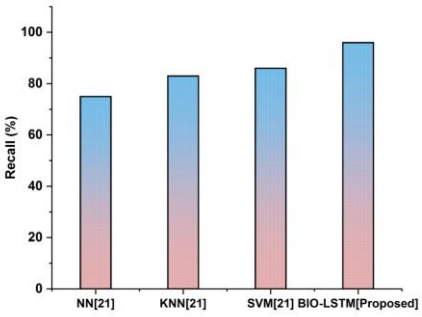

Fig. 7. Results of recall

Table 4. Numerical outcome of recall

	Recall (%)
NN[21]	75
KNN[21]	83
SVM[21]	86
BIO-LSTM[Proposed]	96

The harmonic mean of the proposed model is computed to merge "recall and precision" into a single component called the f1-score. The f1-score is calculated using equation (12).

$$\text{F1} - \text{score} = \frac{(\text{precision}) \times (\text{recall}) \times 2}{\text{precision+recall}} \quad (12)$$

In Fig. 8, BIO-LSTM scored (70.93%) on the f1-score, followed by KNN (60.19%), SVM (80.67%), and NN (86.23%).

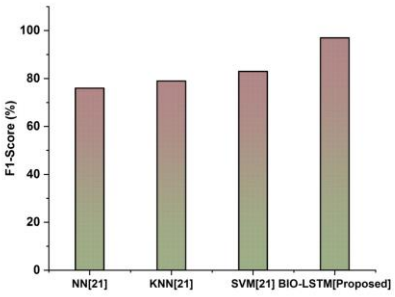

Fig. 8. Results of f1-score

Table 5. Numerical outcome of f1-score

	F1-Score (%)
NN[21]	76
KNN[21]	79
SVM[21]	83
BIO-LSTM[Proposed]	97

Specificity is the ability to assess the substance in the condition of elements that could be predicted to be present. The ratio between the value of TNs and the sum of TNs and FPs is a general understanding of specificity. The specificity is calculated using equation (13).

$$\text{specificity} = \frac{\text{TN}}{\text{TN+FP}} \quad (13)$$

In Fig. 9, the Specificity for KNN is 62.55%, K-means is 80.97%, CNN is 72.36%, and MA-CNN is 87.98%.

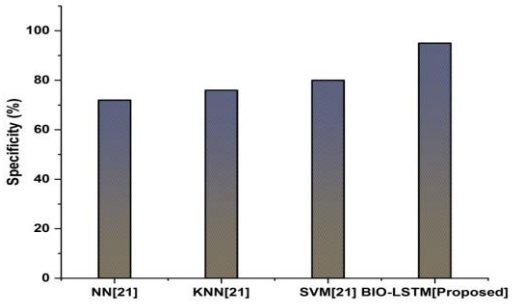

Fig. 9. Results of specificity

Table 6. Numerical outcome of specificity

	Specificity (%)
NN[21]	72
KNN[21]	76
SVM[21]	80
BIO-LSTM[Proposed]	95

5. Conclusion

In this work, a new method for combining a combination of BIO-LSTM approaches to detect pneumonia in images from chest X-rays is proposed. CXR images were compiled into a comprehensive Kaggle dataset from many sources. To provide an accurate portrayal of the target pathophysiology, the dataset included a wide variety of pneumonia and non-pneumonia patients. The dataset was processed utilizing SAE methods to enhance its quality and utility. Utilizing the Gabor filter to feature extraction. A dataset of chest X-rays including both normal and pneumonia patients are used to assess the suggested approach. Experimental findings show that the BIO-LSTM methodology outperforms more conventional approaches in terms of performance. The results of this investigation indicate that BIO-LSTM is combined. The method may help doctors identify patients more quickly and accurately, improving patient outcomes and lowering healthcare costs in the process.

References

[1] Kong, L., Ren, Z., Zhou, Y., Ding, W. and Cheng, J., 2022, June. Research on Medical Image Classification Based on Image Segmentation and Feature Fusion. In Proceedings of the 6th International Conference on High Performance Compilation, Computing and Communications (pp. 150-155).

[2] Rajpal, S., Lakhyani, N., Singh, A.K., Kohli, R. and Kumar, N., 2021. Using handpicked features in conjunction with ResNet-50 for improved detection of COVID-19 from chest X-ray images. Chaos, Solitons & Fractals, 145, p.110749.

[3] Christina Magneta, S., Sundar, C. and Thanabal, M.S., 2023. Lung lobe segmentation and feature extraction-based hierarchical attention network for COVID-19 prediction from chest X-ray images. The Computer Journal, 66(2), pp.508-522.

[4] Ukwuoma, C.C., Qin, Z., Heyat, M.B.B., Akhtar, F., Smahi, A., Jackson, J.K., Furqan Qadri, S., Muaad, A.Y., Monday, H.N. and Nneji, G.U., 2022. Automated Lung-Related Pneumonia and COVID-19 Detection Based on Novel Feature Extraction Framework and Vision Transformer Approaches Using Chest X-ray Images. Bioengineering, 9(11), p.709.

[5] Baghdadi, N.A., Malki, A., Abdelaliem, S.F., Balaha, H.M., Badawy, M. and Elhosseini, M., 2022. An automated diagnosis and classification of COVID-19 from chest CT images using a transfer learning-based convolutional neural network. Computers in biology and medicine, 144, p.105383.

[6] Ahmadian, S., Jalali, S.M.J., Islam, S.M.S., Khosravi, A., Fazli, E. and Nahavandi, S., 2021. A novel deep neuroevolution-based image classification method to diagnose coronavirus disease (COVID-19). Computers in biology and medicine, 139, p.104994.

[7] Farhan, A.M.Q. and Yang, S., 2023. Automatic lung disease classification from the chest X-ray images using hybrid deep learning algorithm. Multimedia Tools and Applications, pp.1-27.

[8] Lakshman Narayana, V., Lakshmi Patibandla, R.S.M., Pavani, V. and Radhika, P., 2022. Optimized Nature-Inspired Computing Algorithms for Lung Disorder Detection. In Nature-Inspired Intelligent Computing Techniques in Bioinformatics (pp. 103-118). Singapore: Springer Nature Singapore.

[9] Jalali, S.M.J., Ahmadian, M., Ahmadian, S., Hedjam, R., Khosravi, A. and Nahavandi, S., 2022. X-ray image based COVID-19 detection using evolutionary deep learning approach. Expert Systems with Applications, 201, p.116942.

[10] Narula, A. and Vaegae, N.K., 2023. Development of CNN-LSTM combinational architecture for COVID-19 detection. Journal of Ambient Intelligence and Humanized Computing, 14(3), pp.2645-2656.

[11] Shankar, K., Perumal, E., Díaz, V.G., Tiwari, P., Gupta, D., Saudagar, A.K.J. and Muhammad, K., 2021. An optimal cascaded recurrent neural network for intelligent COVID-19 detection using Chest X-ray images. Applied soft computing, 113, p.107878.

[12] Anter, A.M., Oliva, D., Thakare, A. and Zhang, Z., 2021. AFCM-LSMA: New intelligent model based on Lévy slime mould algorithm and adaptive fuzzy C-means for identification of COVID-19 infection from chest X-ray images. Advanced Engineering Informatics, 49, p.101317.

[13] Muhammad, U., Hoque, M.Z., Oussalah, M., Keskinarkaus, A., Seppänen, T. and Sarder, P., 2022. SAM: Self-augmentation mechanism for COVID-19 detection using chest X-ray images. Knowledge-Based Systems, 241, p.108207.

[14] Kong, L. and Cheng, J., 2021. Based on improved deep convolutional neural network model pneumonia image classification. PloS one, 16(11), p.e0258804.

[15] Shankar, K., Perumal, E., Tiwari, P., Shorfuzzaman, M. and Gupta, D., 2022. Deep learning and evolutionary intelligence with fusion-based feature extraction for detection of COVID-19 from chest X-ray images. Multimedia Systems, 28(4), pp.1175-1187.

[16] Goyal, S. and Singh, R., 2021. Detection and

classification of lung diseases for pneumonia and Covid-19 using machine and deep learning techniques. Journal of Ambient Intelligence and Humanized Computing, pp.1-21.

[17] Das, A., 2022. Adaptive UNet-based lung segmentation and ensemble learning with CNN-based deep features for automated COVID-19 diagnosis. Multimedia Tools and Applications, 81(4), pp.5407-5441.

[18] Ukwuoma, C.C., Qin, Z., Heyat, M.B.B., Akhtar, F., Bamisile, O., Muaad, A.Y., Addo, D. and Al-Antari, M.A., 2022. A hybrid explainable ensemble transformer encoder for pneumonia identification from chest X-ray images. Journal of Advanced Research.

[19] Pradhan, A.K., Mishra, D., Das, K., Obaidat, M.S. and Kumar, M., 2023. A COVID-19 X-ray image classification model based on an enhanced convolutional neural network and hill climbing algorithms. Multimedia Tools and Applications, 82(9), pp.14219-14237.

[20] Bahgat, W.M., Balaha, H.M., AbdulAzeem, Y. and Badawy, M.M., 2021. An optimized transfer learning-based approach for automatic diagnosis of COVID-19 from chest x-ray images. PeerJ Computer Science, 7, p.e555.

[21] Yee, S.L.K. and Raymond, W.J.K., 2020, September. Pneumonia diagnosis using chest X-ray images and machine learning. In proceedings of the 2020 10th international conference on biomedical engineering and technology (pp. 101-105).

[22] Mr. Kaustubh Patil, Promod Kakade. (2014). Self-Sustained Debacle Repression Using Zig-Bee Communication. International Journal of New Practices in Management and Engineering, 3(04), 05 - 10. Retrieved from http://ijnpme.org/index.php/IJNPME/article/view/32

[23] Dasi , S. ., & Rao, G. M. . (2023). Design and Analysis of Metamaterial Absorber using Split Ring Resonator for Dual Band Terahertz Applications. International Journal on Recent and Innovation Trends in Computing and Communication, 11(1), 128–132. https://doi.org/10.17762/ijritcc.v11i1.6059